# Characterization of Thin Film Boron Nitride Coatings and Observation of Graphite-Like Boron Nitride

G. Durkaya[a,*], İ. Efeoğlu[b], K. Ersoy[c], B. Çetin[c] and H. Kurtuldu[d]

[a]Atilim University, Department of Metallurgical and Materials Engineering, Ankara, Turkey
[b]Atatürk University, Dept. of Mechanical Engineering, Erzurum, Turkey
[c]FNSS Defense Systems Co. Inc., Engineering and Research Department, Ankara, Turkey
[d]Baskent University, Department of Biomedical Engineering, Ankara, Turkey

Cubic boron nitride is a coating solution to improve wear performances in demanding engineering applications. In order to achieve the best performance from this thin film system, the physical dynamics behind the phase compositions, phonon dynamics, surface quality, interfacial effects and stoichiometric relations should be understood. In this study, for this purpose, physical vapor deposition grown BN thin films were studied in detail using the Raman spectroscopy, atomic force microscopy, and scanning electron microscopy techniques.

## 1. Introduction

In most engineering design applications involving machinery, complex mechanisms etc., with rotary, relative or reciprocating motions, friction/wear properties of contacting surfaces affect the overall performance. One solution is to use high hardness thin film coatings to improve part's performance by reducing the wear effect. A recent candidate, cubic boron nitride (c-BN), is a III–V binary system [1] which has four typical crystal structures: hexagonal, cubic, rhombohedral, and wurtzite. While h-BN exhibits graphite-like properties, c-BN is the hardest material after diamond. Unlike diamond, c-BN is not found in nature and during its formation, BN crystallizes in zinc-blende structure very close to the diamond as $s$ and $p$ orbitals overlap [2]. Physical vapor deposition (PVD) and plasma assisted chemical vapor deposition (PACVD) are the most common techniques to grow c-BN films. Compared to direct current magnetron sputtering (DCMS), high power impulse magnetron sputtering (HiPIMS) provides stoichiometric advantages in PVD growth. Although it has lower growth rate due to low duty cycle, HiPIMS provides lower surface roughness, higher material density, and better hardness performance when it is used simultaneously with DCMS [3]. In this study, BN thin films were grown using HiPIMS PVD on glass and silicon (Si) substrates.

## 2. Experimental procedure

BN films were grown by using HiPIMS with closed field unbalanced magnetron sputtering (CFUBMS by Teer Coating Ltd.) system using Taguchi $L_9$ ($3^3$) design of experiments model. A schematic of the system and BN growth layers are given in Fig. 1a and b, respectively. BN films were grown in two different substrates (silicon (111) and glass) to study film properties. In order to relax the BN lattice by reducing the lattice mismatch between substrate and BN film 4 step buffer layers was used: Ti, TiN, TiB$_2$, TiBN from substrate to BN composite layers: B$_4$C, B4C+B-CN, hBN+cBN. In growth of buffer layers, DCMS method was used and in growth of BN composite HiPIMS method was used for sputtering.
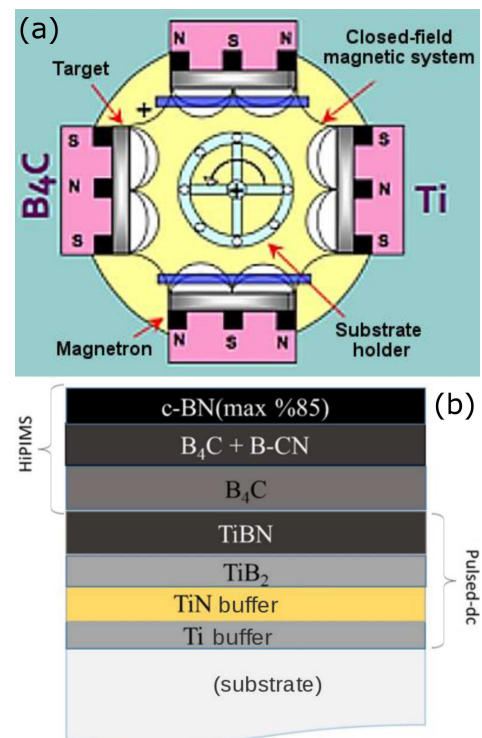


Fig. 1. (a) Schematic of the closed field unbalanced magnetron sputtering system, (b) BN growth layers.

*corresponding author; e-mail:
goksel.durkaya@atilim.edu.tr

BN layers grown on Si and glass substrates were characterized using scanning electron microscopy (SEM), the Raman spectroscopy, and atomic force microscopy (AFM) techniques. SEM images were taken using QUANTA 400F field emission SEM. For the Raman spectroscopy, a homemade Raman spectrometer to record Stokes and anti-Stokes shifts was used with excitation wavelength of 532 nm (BW: 15 nm) and power of 10 mW in back-scattering geometry. AFM topography images were captured with $512 \times 512$ pixels in an area of 5 $\mu$m $\times$5 $\mu$m using a Veeco MultiMode microscope.

## 3. Results and discussion

The SEM image delineated in Fig. 2 was captured at off-angle on a region of the scratched film to analyze the cross-section view of the grown layers. The yellow and red arrows indicate the cascaded Ti, TiN, TiB$_2$, TiBN buffer layers. Yellow arrow shows Ti and TiN buffers while red one shows B rich TiB$_2$ and TiBN buffer layers. The green arrow shows the BN composite film layer.

BN films grown on silicon were analyzed by the Raman spectroscopy. The Raman spectrum in Fig. 3 with the Stokes and anti-Stokes regions shows the Raman lines on both sides of the Rayleigh scattering line. This observation suggests that possible lattice stress might result in intrinsic phonon excitation leading to anti-Stokes shift. The Stokes region of the Raman spectra are analyzed from the same figure. While the 699 cm$^{-1}$ Raman line can be attributed to the TiN TO vibration mode, the vibration of 781 cm$^{-1}$ corresponds to the rhombohedral phase of BN [4]. The vibration at 881 cm$^{-1}$ links to the X-branch of c-BN TO mode. Since it is lower than the values reported in the literature [5], it might be related to layer stresses. The peaks at 1124 and 1071 cm$^{-1}$ correspond to c-BN LO (L) and TO ($\Gamma$) modes, respectively. The vibration at 1291 cm$^{-1}$ can be attributed to LO

($\Gamma$) mode. Particularly, the shifts in the middle of the Brillouin region $\Gamma$ are of great importance in understanding the material since it provides useful information for studying the structure of the Brillouin region in relation to the crystal structure. On the other hand, 1357 cm$^{-1}$ indicates the h-BN $E_{2G}$ mode. This mode is not divided in the LO and TO modes in the hexagonal structure and provides information about the crystal quality. The peak at 1617 cm$^{-1}$ is for C=C vibration and may be due to B$_4$C source. Other high-frequency modes are the modes of the BN phases. As a result, it can be concluded that there are h-BN and r-BN phases besides c-BN.
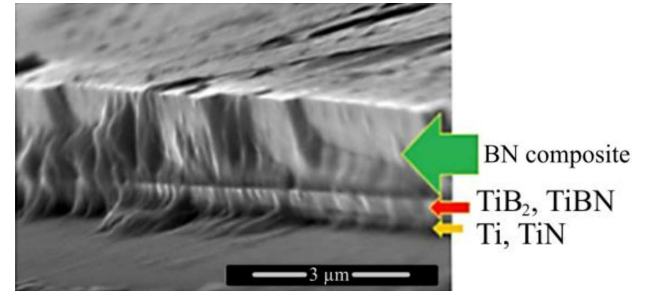


Fig. 2. SEM image showing the cascaded buffer layers (Ti, TiN, TiB$_2$, TiBN) and BN composite film layer. Yellow and red arrows show Ti–TiN and TiB$_2$–TiBN buffer layers, respectively. Green arrow shows BN composite layer. The scale bar is 3 $\mu$m.

AFM measurements were performed on BN layers grown on Si and glass substrates. The roughness values are summarized in Table I. The BN layer grown on Si substrate has a $R_q$ value of 0.57 nm while it is 21.1 nm for the one grown on glass. This indicates Si crystal structure results in better BN crystal form compared to amorphous glass.
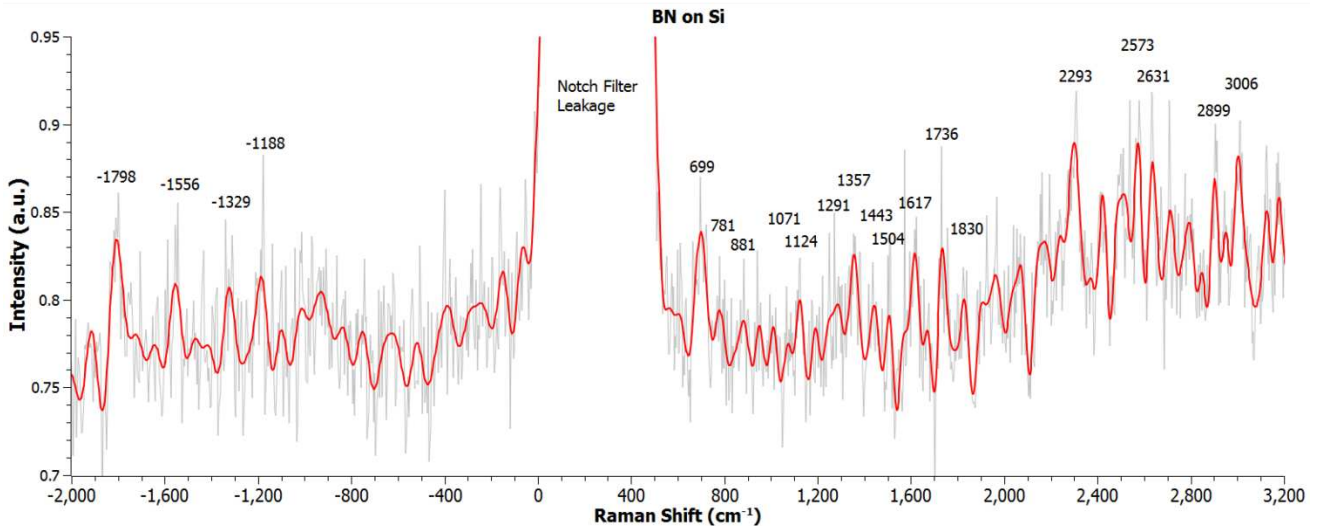


Fig. 3. Raman spectra of BN layer grown on Si substrate. The red curve indicates the Lorentzian peak fitting.

Roughness values based on AFM analysis
of BN/glass and BN/Si layers.

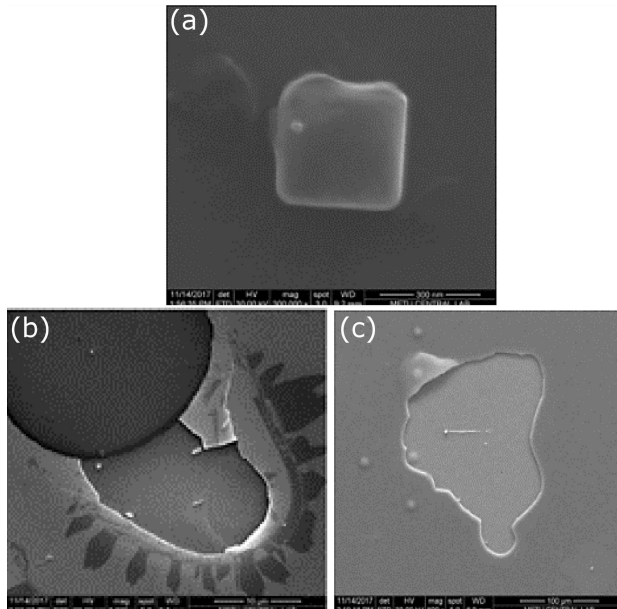| Roughness | BN/glass | BN/Si |
|-----------|----------|-------|
| $R_a$ | 15.5 nm | 0.45 nm |
| $R_q$ | 21.1 nm | 0.57 nm |



Fig. 4. SEM images of BN/Si: (a) c-BN crystal, (b) and (c) examples of surface defects peeled off from the surface. The scale bar represents 300 $\mu$m in (a), 40 $\mu$m in (b), and 100 $\mu$m in (c).

Finally, SEM images of BN layers grown on Si substrates are presented in Fig. 4. Figure 4a shows a bystanding c-BN crystal. Figure 4b and c illustrates some defects peeled off from the surface layer by layer. This is an indication of graphite-like film property and might be expected from h-BN crystal matrix. This could be related to layer by layer growth and covalent bonding structure between inner layers.

## 4. Conclusion

In this study, BN thin films were successfully grown by PVD using HiPIMS sputtering systems. The process was carried out by CFUBMS. The BN layers exhibited cubic, hexagonal, rhombohedral phases, detected by the Raman spectroscopy analysis. The layers grown on Si showed better Raman spectra and yielded higher surface roughness values than the ones grown on glass. According to the SEM analysis, the surface was peeled off layer by layer in a graphite-like manner in addition to the observation of cubic crystal islands. This may open new research avenues to utilize the BN material system in nanotechnology applications.

## Acknowledgments

## References

[1] L. Vel, G. Demazeau, J. Etourneau, *Mater. Sci. Eng. B* **10**, 149 (1991).

[2] G. Will, B. Kiefer, *ZAAC* **627**, 2100 (2001).

[3] S. Schmidt, C. Höglund, J. Jensen, L. Hultman, J. Birch, R. Hall-Wilton, *J. Mater. Sci.* **51**, 10418 (2016).

[4] Lili Yu, Bin Gao, Zhi Chen, Chuantao Sun, Deliang Cui, Chengjian Wang, Qilong Wang, Minhua Jiang, *Chin. Sci. Bull.* **50**, 2827 (2005).

[5] S. Reich, A.C. Ferrari, R. Arenal, A. Loiseau, I. Bello, J. Robertson, *Phys. Rev. B* **71**, 205201 (2005).